CHAPTER 39

Hybrid Domain Decomposition for Configurations with Multiple Nonsimilar Components

Kamran Fouladi[1]
Oktay Baysal[2]
James C. Newman[3]

INTRODUCTION

Domain decomposition techniques (DDT) have become one of the most successful tools used in circumventing problems faced in generating grids about complex configurations. Such configurations may have multiple, joint or disjoint components, all of which may also be geometrically nonsimilar. Each DDT is designed to simplify the grid generation by subdividing the flow domain into simpler subdomains which accept easily constructed grids. Other advantages may be the option to use different solution techniques, or even different forms of the flow equations in different subdomains. Also, since only one subdomain has to reside in the computer core memory, a DDT also reduces the memory requirement.

Popular DDT's include methods such as multiblock grids, zonal grids, and overlapped grids. These methods vary in constructing the grid interfaces and establishing the communication among the subdomain grids. These differences in turn influence the extent that these methods could ensure conservation at grid interfaces. They also affect the flexibility of these methods to consider complex configurations where geometrically nonsimilar components may coexist.

A Hybrid Domain Decomposition (HDD) approach, which is developed to take advantage of each technique's strengths, is proposed in this paper. In deciding on the type of hybridization of techniques for a configuration, two major concerns are the geometry of the configuration and a priori knowledge of the flowfield. A proper choice of hybridization requires a compromise, so that generating each subdomain grid is an easy task, and physical and intergrid boundary conditions can easily be implemented. It also requires that the total number of cells is minimized with proper resolution everywhere, and finally the flux conservation is enforced where significant flow gradients occur.

Some applications of HDD are reported in Refs. 1–3. In these applications, the Navier-Stokes equations are solved on a combination of multiblock and overlapped grids. The first objective of the current study is to illustrate the capability of the current algorithm as it considers all of the aforementioned DDT's. The second objective is to simulate the effects of the wake generated behind the base of a parent body on the aft launched projectile (ALP).

[1]Old Dominion University, Mechanical Engineering and Mechanics Department, Norfolk, VA 23529. Post-doctoral fellow. Presently with Lockheed Engineering & Sciences Co., Hampton, VA.
[2]Old Dominion University, Mechanical Engineering and Mechanics Department, Norfolk, VA 23529. Associate Professor, Member SIAM.
[3]Old Dominion University, Mechanical Engineering and Mechanics Department, Norfolk, VA 23529. Undergraduate Research Assistant.

GOVERNING EQUATIONS AND THEIR SOLUTION

The conservative form of the nondimensional, unsteady, compressible, Reynolds-averaged, complete Navier-Stokes equations are written in the generalized curvilinear coordinates,

$$\frac{\partial \bar{Q}}{\partial t} + \frac{\partial}{\partial \xi^m}\left(\bar{E} - \bar{E}_v\right)_m = 0; \qquad m = 1,2,3 \tag{1}$$

where

$$\bar{Q} = [\rho, \rho u_1, \rho u_2, \rho u_3, \rho e]^T / J \tag{2}$$

The symbols t, ρ, u, e, p denote the time, density, Cartesian velocity components, internal energy, and pressure, respectively. The fluxes of the conserved variables are

$$\bar{E}_m = \frac{1}{J}[\rho U_m, \rho u_1 U_m + \partial_1 \xi^m p, \rho u_2 U_m + \partial_2 \xi^m p, \rho u_3 U_m + \partial_3 \xi^m p, \rho U_m h]^t \tag{3}$$

$$\left(\bar{E}_v\right)_m = \frac{1}{J}[0, \partial_k \xi^m \tau_{k1}, \partial_k \xi^m \tau_{k2}, \partial_k \xi^m \tau_{k3}, \partial_k \xi^m (u_r \tau_{kr} - q_k)]^t \tag{4}$$

$$U_m = \partial_k \xi^m u_k \tag{5}$$

The symbols U, h, τ, q denote the contravariant velocity, enthalpy, shear stress, and heat flux, respectively.

$$\partial_k \xi^m \tau_{k1} = \frac{M_\infty \mu}{Re}\left[\left(\partial_k \xi^m \partial_1 \xi^r - \frac{2}{3}\partial_1 \xi^m \partial_k \xi^r\right)\frac{\partial u_k}{\partial \xi^r} + \partial_k \xi^m \partial_k \xi^r \frac{\partial u_1}{\partial \xi^r}\right]. \tag{6}$$

The expressions for $(\partial_k \xi^m \tau_{k2})$ and $(\partial_k \xi^m \tau_{k3})$ are obtained analogous to Eq. (6) with the subscript 1 replaced by 2 and 3, respectively.

$$\partial_k \xi^m q_k = \frac{M_\infty \mu}{Re \cdot Pr} \frac{1}{(1-\gamma)} \partial_k \xi^m \frac{\partial T}{\partial \xi^r} \tag{7}$$

The molecular viscosity is calculated from the Sutherland's law. The state equations are written by assuming air to be a perfect gas,

$$p = \rho(\gamma - 1)\left(e - \frac{U^2}{2}\right) \tag{8}$$

$$h = \frac{\gamma p}{\rho(\gamma - 1)} + \frac{U^2}{2} \tag{9}$$

The symbols γ, T, μ, Re, M, Pr denote the ratio of specific heats, temperature, viscosity coefficient, Reynolds, Mach, and Prandtl numbers, respectively. J is the transformation Jacobian and m, k, r are dummy indices. A repeated index in a term implies a summation.

An option is built in the computations to invoke the thin-layer approximation (Ref. 1) in any direction (ξ^1, ξ^2 or ξ^3). This is particularly beneficial when incorporated with domain decomposition techniques, since such different flow governing equations can be used for different subdomains. In this study, the option is invoked to solve the thin-layer approximation of Navier-Stokes equations in two different directions on two separate subdomains.

Equation (1) is solved using the implicit, finite volume, and spatially second-order accurate method described in Refs. (1–6). Roe's flux-difference splitting (FDS) is used to construct the upwind differences for the convective and pressure terms. Spatial derivatives are written conservatively as flux balances across the cells of this finite volume formulation. The diffusion terms are centrally differenced. Spatial approximate factorization, and Euler backward integration after linearization in time, result in the solution through 5×5 block-tridiagonal matrix inversions in each of the three directions. When an upwind-biased approximation scheme is used, numerical oscillations are expected to appear in the presence of discontinuities. A flux limiter can be used to reduce an upwind-biased difference to a fully one-sided upwind scheme in such regions. This in turn ensures a monotonic interpolation and eliminates the overshoots and the undershoots. In the present formulation, the min-mod type flux limiter (Ref. 6) is used to control oscillations in the vicinity of large gradients.

Hybrid Domain Decomposition

A composite grid for a flow domain consists of any combination of the popular domain decomposition techniques. The composite grid for the present demonstrative case is shown in Fig. 1. Grids 1 and 2 are zonally patched, Grids 2 and 3 are multiblock structured, and Grid 4 is overlapped on Grid 2. The details of each DDT can be found in, for example, Refs. 1–3 and 7–10.

The multiblock structured grids (Ref. 7) are easy to generate but lack the geometrical flexibility. This DDT allows any number of blocks to be employed to fill an arbitrary three-dimensional region without holes or overlaps. Any block can be linked to any other block subject to the constraint that the grid lines normal to the interfaces need to be contiguous. Hence, interpolations are not necessary at these interfaces. The conservation across these interfaces is ensured through matching the solutions by using two cells of the neighboring grid as boundary cells.

The zonal method, also known as grid patching (Refs. 8, 9), requires the domain to be divided into subdomains with simple and easily generated grids. These grids are then patched together along common surfaces. Unlike the multiblock grids, the grid lines in adjacent grids are not aligned with each other at the grid interfaces. The zonal method is shown to be conservative except across surfaces with high curvature. Ensuring conservation across these surfaces is not theoretically impossible, but it is rather difficult to obtain.

In the zonal approach, any given surface, say the ξ^1 = constant surface, is discretized in two different sets of cell faces since two grids meet along this surface. The zonal patching of Grids 1 and 2 (Fig. 1) is detailed in Fig. 2 as an example. The grids meet at the cross section of the parent body's base. The H-O type Grid 2 (33×69) is patched longitudinally downstream of the H-O type Grid 1 (29×41), which wraps around the parent body. Grid 2 is much finer and it is used to analyze the complicated wake flow generated by the parent body. It also serves as the global grid which contains the overlapped Grid 4 of the projectile. In order to ensure conservation across a zonal interface, the surface integral taken on the interface must be equal to a constant with both Grid 1 and Grid 2 data. Using a superscript to indicate the grid number, the conservation requirement on a constant ξ^1 surface (discretized with $J \times K$ grid lines) becomes

$$\sum_{j^1}^{J^1}\sum_{k^1}^{K^1}[E\Delta S]_{j^1,k^1} = \sum_{j^2}^{J^2}\sum_{k^2}^{K^2}[E\Delta S]_{j^2,k^2} \tag{10}$$

where ΔS is the actual area of each cell face.

This constraint ensures flux conservation across the zonal interface and it does not restrict the local transport of flux from a single cell to another cell across the patched grid boundary. That is, Eq. (10) does not provide a unique formula to construct the flux distribution of $E_{j,k}$ of Grid 2, if $E_{j,k}$ of Grid 1 as well as values of ΔS in both zones are provided. This can be accomplished by enforcing conservation on a local (cell-to-cell) level. Conservation on the (j^2, k^2) cell face requires that

$$[E\Delta S]_{j^2,k^2} = \int\int_{\Delta S_{j^2,k^2}} [(E\cdot n)ds]^1 \tag{11}$$

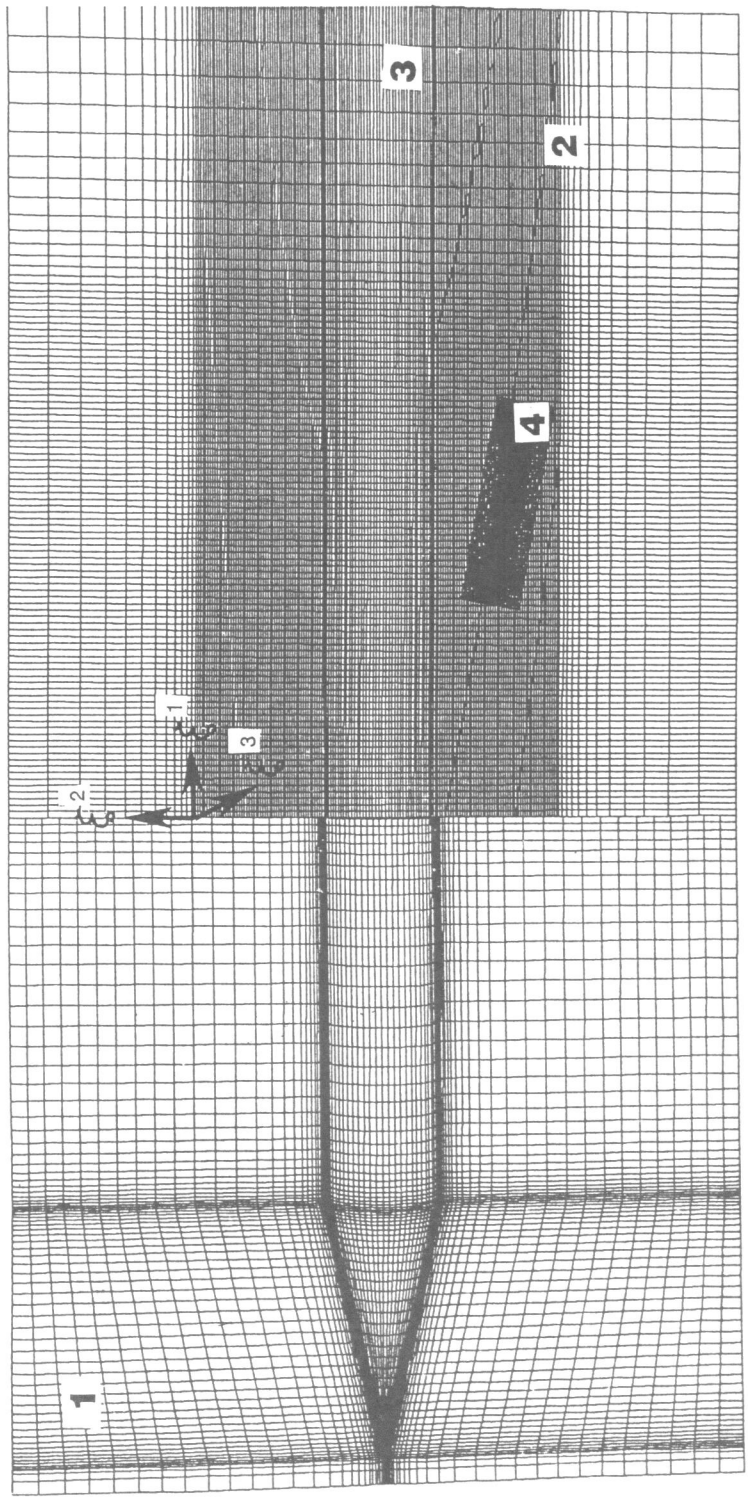

Fig. 1 The composite grid for the parent body and the aft launched projectile (ALP) configuration. Grid 1/Grid 2 interaction is zonal, Grid 2/Grid 3 interaction is multiblock structured, and Grid 2/Grid 4 interaction is overlapped.

Fig. 2 The detail of the zonal intersection; (a) the cross section of Grid 1, (b) the cross section of Grid 2.

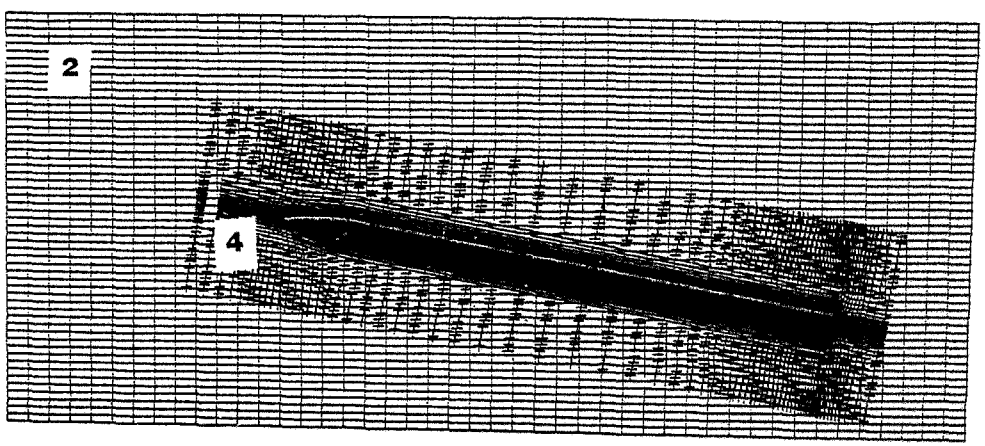

Fig. 3 The detail of the overlapped grids at the longitudinal symmetry plane. (+) symbols indicate the region where the solution is obtained on both Grids 2 and 4, then interpolated trilinearly.

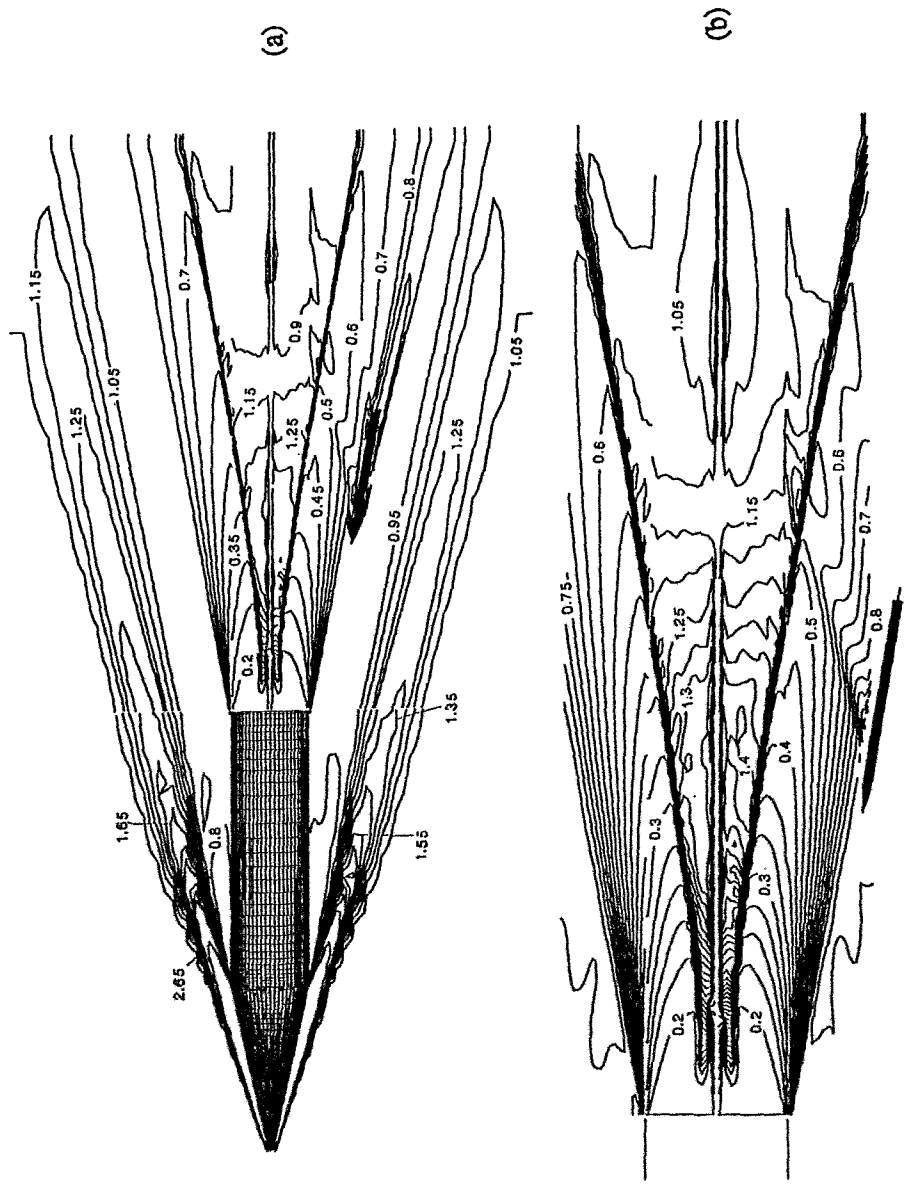

Fig. 4 (a) The normalized pressure contours at the longitudinal symmetry plane; (b) the enlarged view of the wake region.

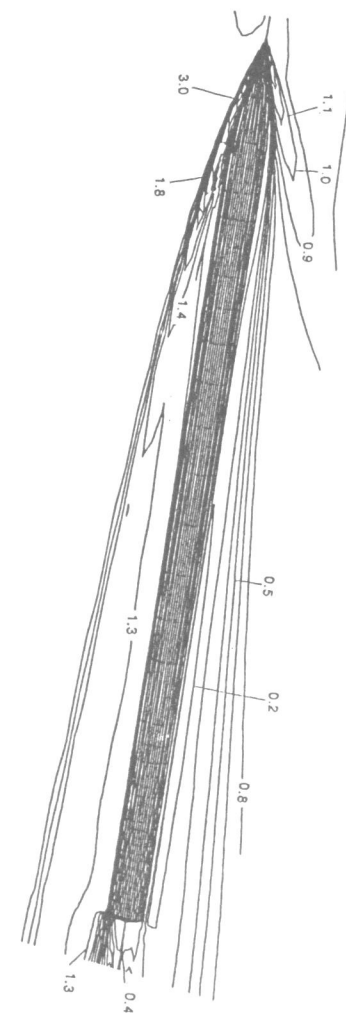

Fig. 5 The density contours at the longitudinal symmetry plane of the projectile.

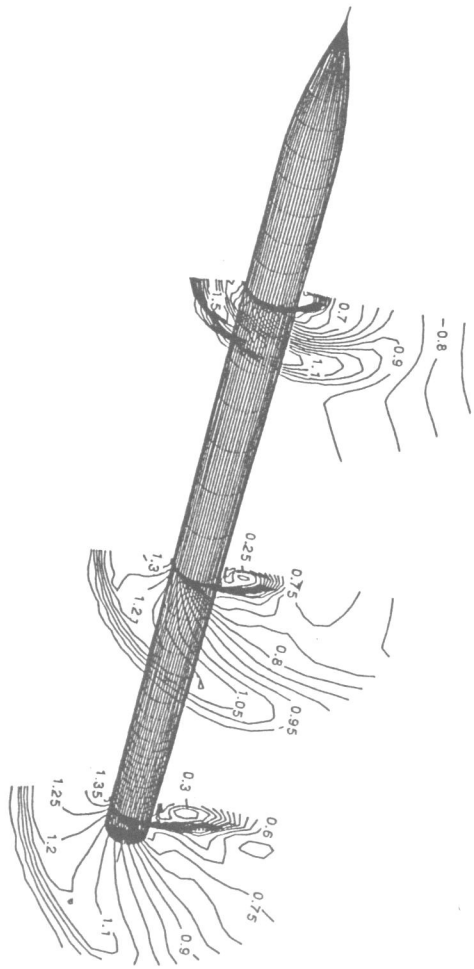

Fig. 6 The density contours at three crossflow planes of the projectile.

The integration on the right side of the above equation extends over the quadilateral cell face in Grid 2, but the integrand is based on Grid 1 data.

In contrast to multiblock and zonal grids, the grid overlapping method does not require common boundaries among its subdomains. Matching the solution across the boundaries is provided by a common or overlapped region. Each subdomain in a composite of overlapped grids may have a grid with a different topology. A drawback of overlapped grids is the difficulty in constructing the conservative transfer of fluxes across the interfaces. The details of this method are given in Ref. 10 for two dimensions, and in Refs. 1–3 for a three-dimensional, multigrid, finite volume algorithm. Shown in Fig. 3 is the overlapped grids detail (Grids 2 and 4) of the present demonstrative example. (+) symbols indicate the overlapped region, where the solution from one grid is interpolated to the other.

RESULTS

It is often of interest to study a flow past more than one object, where the interference effects become important. An example is the aft launched projectile (ALP) problem. The parent body (Fig. 1) is a cone nosed cylinder with a 6.0 in. base diameter and it is positioned at 0° angle of attack (AOA). Its length is 35.0 in. including the 13.5 in. forebody. ALP (Fig. 3) is an ogive nose cylinder with 0.4 in. base diameter and it is at 10° AOA. Its length is 9.5 in. including the 1.2 in. forebody. The horizontal and vertical distances from the center of the parent body base to the ALP nose are 11.5 in. and 6.0 in., respectively. The freestream flow Mach number is 5.0 and the Reynolds number is 1.0×10^6 based on the parent body diameter. The flow is assumed symmetric, and hence the grid is generated for circumferentially half bodies. The total number of cells in the four subdomain grids used for the computations (Fig. 1) is 461,684.

Presented in Figs. 4–6 are the preliminary results for the numerically simulated flowfield. The normalized pressure (the freestream value is unity) contours of the longitudinal symmetry plane (Fig. 4a) depict the attached nose shock, the expansion at the forebody junction, and the parent body wake. This wake includes a strong base shock generated due to the overexpansion of the flow at the edge of the base. The contour lines cross the Grid 1/Grid 2 interface smoothly. This is expected of the zonal method, where the flow fluxes are transferred conservatively. The enlarged view of the wake is shown in Fig. 4b. The upstream pressure for ALP is 0.9 rather than the freestream value of 1.0. Despite the nonconservative flux transfers, the contour lines cross the Grid 2/Grid 4 interface rather smoothly. The symmetry of the parent body wake is altered due to the interference. The effect of the ALP nose shock on the wake manifests itself in increased pressure values. The contours crossing the Grid 2/Grid 3 interface, where the multiblock grid technique is used, do not appear to feel the existence of such an interface.

The ALP flowfield is further detailed via the normalized density contours of the symmetry plane (Fig. 5) and three crossflow planes (Fig. 6). The ALP nose shock is followed by the expansions along its forebody. As expected, leeside vortices are formed and their sizes grow in the axial direction as the influence of the crossflow increases.

CONCLUSIONS

A hybrid domain decomposition (HDD) method is developed and illustrated through an example problem. This example problem is rather challenging, since the flowfield includes two strong nose shocks and a strong base flow shock. The present HDD formulation combines the advantages of the individual DDT's in a judicious manner. The multiblock and the zonal methods are flux conserving, but the overlapped grids method is nonconservative.

Preliminary results are obtained for the high speed flow past an aft launched projectile (ALP) in its parent body wake. It would be rather difficult to generate a single grid for this flowfield. This HDD method should prove to be even more useful, when solutions are needed for a series of ALP locations and positions, since the subdomain grids are reusable.

ACKNOWLEDGMENT

This work is supported jointly by USAF Armament Laboratory, Eglin AFB, FL. and NASA Langley Research Center, Hampton, VA. The technical monitors are Dr. L. Bruce Simpson and David S. Miller.

REFERENCES

1. Baysal, O., Fouladi, K., Lessard, V. R., "Multigrid and Upwind Viscous Flow Solver on 3–D Overlapped and Embedded Grids," AIAA Paper No. 89–0464, January 1989. Also, AIAA Journal, Vol. 29, No. 4, April 1991.

2. Fouladi, K., Baysal, O., "Viscous Simulation Method for Unsteady Flows Past a Configuration with Nonsimilar Multicomponents," Recent Advances and Applications in CFD (Ed.: O. Baysal), ASME-FED, Vol. 103, Winter Annual Meeting, November 1990, pp. 181–190. Also, to appear in Journal of Fluids Engineering.

3. Baysal, O., Fouladi, K., Leung, R. W., Sheftic, J. S., "Viscous Analysis of Interference Flows Past Cylinder-Fin-Sting Assemblies Near Cavities," AIAA Paper No. 90–3095 CP, Proceedings of 8th Applied Aerodynamics Conference, August 1990, pp. 884–892. Also, to appear in (AIAA) Journal of Aircraft.

4. Thomas, J. L., Taylor, S. L., Anderson, W. K., "Navier-Stokes Computations of Vortical Flows Over Low Aspect Ratio Wings," AIAA Paper No. 87–0207, January 1987.

5. Baysal, O., Fouladi, K., Miller, D. S, "Computation of Supersonic Flows Over a Body at High Angles of Attack," AIAA Journal, Vol. 27, No. 4, pp. 427–437, April 1989.

6. Anderson, W. K., Thomas, J. L., Van Leer, B., "Comparison of Finite Volume Flux Splitting Methods for the Euler Equations," AIAA Journal, Vol. 24, No. 9, September 1986, pp. 1453–1460.

7. Thompson, J. F., "A Composite Grid Generation Code for General Three-Dimensional Regions," AIAA-87–0275, January 1987.

8. Walters, R. W., Reu, T., McGrory, W. D., Thomas, J. L., Richardson, P. F., "A Longitudinally-Patched Grid Approach with Applications to High Speed Flows," AIAA Paper No. 88–0715, January 1988.

9. Thomas, J. L., Walters, R. W., Reu, T., Ghaffari, F., Weston, R. P., Luckring, J. M., "A Patched-Grid Algorithm for Complex Configurations Directed Toward the F/A-18 Aircraft," AIAA Paper No. 89–0121, January 1989.

10. Steger, J. L., Dougherty, F. C., Benek, J. A., "A Chimera Grid Scheme," Advances in Grid Generation (Ed.: K. Ghia), ASME-FED, Vol 5, June 1983, pp. 59–69.